Pre-Print Manuscript of Article:

Bridgelall, R., Rahman, M. T., Tolliver, D. D., Daleiden, J. F., "Wavelength sensitivity of a connected vehicle method of ride quality characterizations," *International Journal of Pavement Engineering*, pp. 1-7, April 18, 2017, DOI: 10.1080/10298436.2017.1316645.

Wavelength sensitivity of roughness measurements using connected vehicles

Researchers previously demonstrated that a roughness index called the road impact factor (RIF) is directly proportional to the international roughness index (IRI) when measured under identical conditions. A RIF-transform converts inertial signals from connected vehicle accelerometers and speed sensors to produce RIF-indices in real-time. This research examines the relative sensitivities of the RIF and the IRI to variations in dominant profile wavelengths. The findings are that both indices characterize roughness from spatial wavelengths up to 2 meters with equal sensitivity. However, the RIF transform maintains its sensitivity when characterizing roughness from wavelengths beyond that. The case studies used a certified inertial profiler to collect both RIF and IRI data simultaneously from five different pavement surface types. The RIF/IRI proportionality factors distributed normally among the profiles tested. This result affirms that the RIF and IRI generally agrees. However, differences in the dominant profile wavelength among pavements will produce some spread in the degree of roughness that the indices express.

Keywords: connected vehicle; inertial profiler; intelligent transportation systems; pavement management; probe vehicles; ride quality; roughness index; wavelength sensitivity

1 Introduction

Transportation agencies rely on the regular reporting of pavement performance to prioritize maintenance needs. As surfaces deteriorate, the induced dynamic loading from heavy vehicles further accelerates road deterioration (Bilodeau, Gagnon and Doré 2015). Current research affirms that smoother roads would lead to a significant improvement in energy consumption (Ghosh *et al.* 2015, Akbarian et al. 2015, Louhghalam, Tootkaboni and Ulm

2015), a reduction in greenhouse gas emissions (González 2016, Louhghalam, Akbarian, and Ulm 2017), and less freight damage (Steyn *et al.* 2015). Existing methods that characterize roughness using the international roughness index (IRI) are difficult or impractical to apply to unpaved, urban, and local roads (Karamihas 2016). These deficiencies, coupled with the relatively high cost to acquire, maintain, and operate inertial profiling equipment, have motivated the development of more affordable methods that can characterize roughness more frequently for the entire network. In particular, the authors previously demonstrated a mathematical transform that operates in real-time, directly on accelerometers signals from connected vehicles (CVs) to produce the road impact factor (RIF) index (Bridgelall *et al.* 2016a, Bridgelall *et al.* 2016b). The authors showed in detail that the RIF-index is directly proportional to the international roughness index (IRI) when measured under identical conditions (Bridgelall 2014a). Those conditions include speed, vehicle suspension, and profile characteristics.

The direct proportionality relationship between RIF-indices and the IRI enables unbiased estimation of one from the other. This ability will benefit agencies that wish to estimate ride quality from connected vehicle data, and to extend deterioration-forecasting models that can utilize both historical IRI data and future CV measurements of RIF-indices. Another important benefit is that agencies can measure RIF-indices for facilities where it is impractical or unaffordable to obtain the IRI with inertial profilers. For example, practitioners can use historical averages of RIF/IRI (R/I) factors to estimate the IRI for local and unpaved roads simply by dividing the measured RIF-indices by the average R/I factor. However, when converting between the two roughness indices, practitioners must take measurements at the same speed as that of the R/I factors available. That is, the speed

dependency of both the IRI- and RIF-transforms affects the R/I factors, even when using the same vehicle.

The main contributions of this paper are to:

(1) Demonstrate the use of a bump function to simulate dominant profile wavelengths, and

(2) characterize the relative sensitivities of the IRI and RIF transforms to dominant profile wavelengths.

Work from previous research showed that it is possible to estimate the IRI from inertial sensors by training artificial neural networks (Dawkins *et al.* 2011), fitting linear regression models to the data (Cruz and Castro 2015), and calibrating inverse state-space models with vehicle suspension parameters (Islam et al. 2016). Other related research mined inertial data from smartphones to identify roadway anomalies (Yi, Chuang and Nian 2015, Akinwande et al. 2015).

The next section reviews the RIF-transform and its direct proportionality relationship with the IRI as a function of traversal speed. The theories introduced explain their sensitivities to variations in the dominant profile wavelengths. Subsequently, case studies of five different pavement types characterize the spreads in R/I factors. The results and discussion section describe the anticipated R/I trends and proposes further research to guide future applications.

2 Methods

The authors provided details of the RIF-transform derivations previous research (Bridgelall 2014a). In those works, the authors also introduced and described the benefits of using modified Gaussian radial bases functions to model bumps of parameterized heights and

widths. The simulated traversal of a spatially defined radial bases function at some speed produces a temporal radial basis function. Subsequently, a Fourier Transform of the temporal function provides its frequency composition. The analysis in this work refers to the frequency of the Fourier Transform peak as the dominant wavelength of the analytical bump.

As also detailed in previous research (Bridgelall 2014a), a combination of bumps with random variations in height and width provides a suitable model for simulating excitations from roadway elevation profiles, without producing discontinuities. Therefore, the Fourier Transform of the temporal profile at some traversal speed will produce a spectrum that represents the intensity of roadway excitations for some span of frequencies. Subsequently, applying the IRI- and the RIF-transforms to the reference quarter-car responses at specified speeds will produce the respective roughness indices. Given the detailed derivations of the RIF-transform and the bump functions cited from the previous work, this section will provide only brief reviews.

2.1 The RIF-Transform

The RIF transform produces a RIF-index in units of g-force per meter to characterize the actual roughness experienced in the sensing vehicle, at any speed. For individual vehicle traversals, the RIF-transform summarizes roughness such that

$$R_{\bar{v}}^{L} = \sqrt{\frac{1}{L}\sum_{n=0}^{N-1}\left|g_{z[n]}v_n\right|^2 \delta t} \tag{1}$$

where the RIF-index $R_{\bar{v}}^{L}$ is the average g-force magnitude experienced per unit of distance

L traveled (Bridgelall *et al*. 2016a). An on-board accelerometer produces the vertical acceleration $g_{z[n]}$ for signal sample n and a speed sensor produces the instantaneous traversal speed v_n. Previous research established that the sample rate, which is the inverse of the average sample period δt, should be at least 64 Hertz (Bridgelall 2014b).

From equation (1), it is evident the RIF-index, which is the output of the RIF-transform, is directly proportional to the vertical acceleration intensity at any fixed speed. By inspection, setting the speed and the segment length to a constant yields the root-mean-square (RMS) of the vertical acceleration, multiplied by a constant. Therefore, by definition of the RMS, the output must be directly proportional to the input.

The IRI is valid only at 80 km h^{-1}. Therefore, any comparison with the RIF-index will require that the RIF-transform use a fixed speed, which may be any speed that users predominantly travel the segment.

2.2 The IRI procedure

The IRI is an estimate of roughness based on the simulated response of a specific quarter-car traversing samples of the measured elevation profile (Gillespie, Sayers and Queiroz 1986). The simulated traversal speed is precisely $\bar{v} = 80$ km h^{-1} (~50 mph) and the quarter-car is a fixed and simplified vehicle model called the Golden Car. The IRI procedure computes the sprung-mass $\dot{z}_s(t)$ and the unsprung-mass $\dot{z}_u(t)$ responses by solving simultaneous differential equations of spring motions. Subsequently, the IRI, denoted $I_{\bar{v}}^{L}$ is the accumulated absolute rate difference between the sprung- and the unsprung-mass motions for a specified traversal distance L such that

$$I_{\bar{v}}^{L} = \frac{1}{L}\int_{0}^{L/\bar{v}} \left|\dot{z}_s(t) - \dot{z}_u(t)\right| dt. \tag{2}$$

In contrast, the RIF-transform operates on the vertical acceleration magnitude resulting from traversals at any specified speed. Therefore, the RIF-index is a magnitude representation of the *measured* g-forces that riders experience while traveling within some speed band. On the other hand, the IRI is an accumulation of the *simulated* vertical motions of a simplified vehicle model moving at a precise speed.

The spatial wavelength composition among pavements differ (Lak, Degrande and Lombaert 2011). Furthermore, different traversal speeds translate spatial wavelengths to temporal wavelengths that excite the actual vibration modes of the vehicle suspension systems. Therefore, the fixed vibration modes of the Golden Car and the precise reference speed of the IRI procedure produce a wavelength bias (Papagiannakis 1997) that mischaracterizes roughness experienced at other speeds. Furthermore, the IRI does not characterize the impact of wheelbases whereas a direct measurement of roughness via g-forces will.

2.3 Direct proportionality relationship

The IRI- and RIF-transforms integrate motion excitation from all vibration frequencies that traversals of an elevation profile might induce. Both transforms produce indices that are directly proportional to the intensity of their input vibrations. This means that for any fixed traversal speed, a linear increase in the height of a bump will produce a linear increase in the respective roughness indices. To illustrate this fact, figure 1 plots the RIF-index and the IRI derived from the vibration responses of a Golden Car simulated to traverse a 2-meter wide bump of varying heights. As demonstrated previously, the direct proportionality of the

RIF-index to the vertical acceleration intensity is also observable by reducing equation (1) to the RMS of the g-forces at a fixed speed.

The output slopes in figure 1 are constants. Therefore, the theoretical R/I factors must be constant for a fixed-width bump of any height, when traversed at a fixed speed. It is evident that the direct proportionality relationship with vibration intensity holds at any fixed traversal speed. For example as shown in figure 1, the RIF-transform at half the IRI reference speed (40 km h^{-1}) produces a lower but constant slope.

[Figure 1 near here].

The random combination of different width bumps produces a theoretical elevation profile that excites the quarter-car response modes. Hence, using the same vehicle at a fixed speed to measure RIF-indices from the same pavement profile must produce consistent R/I factors. The spread in R/I factor measurements will reflect variations in speed, wheel-path, and suspension responses.

2.4 Wavelength sensitivities

As mentioned previously, different traversal speeds translate the waviness of a spatial profile to temporal vibrations at *different* frequencies. The Golden Car dynamic response function varies with temporal vibration frequency to produce different vertical acceleration (g-force) intensities at the different traversal speeds. For example, figure 2(a) illustrates the simulated g-forces of the Golden Car sprung-mass response to the traversal of a 10-meter wide bump at the IRI reference speed. Figure 2(b) illustrates the simulated response from traversing a narrower (2-meter) bump at the same speed.

[Figure 2 near here].

The simulation isolates the bumps such that their peaks are located 80-meters from the beginning of an otherwise smooth elevation profile. That is, the g-force is zero prior to arriving at the bump. The damping characteristics of the Golden Car dissipate the transient responses from both bump traversals within approximately one second or equivalently after about 20 meters of travel at the IRI reference speed. Although the heights of each bump (2-centimeters) are identical and the traversal speed is unchanged, the narrower bump induces a higher intensity vibration response. The dominant frequency also increases.

Figure 3 plots the frequency spectra of the wide bump (black solid line) and the narrow bump (solid grey line) relative to the Golden Car response (dashed grey line). The two Golden Car response peaks are located at its sprung mass mode (1.3 Hertz) and unsprung mass mode (10.5 Hertz). As described previously, a Fourier Transform of the temporal bump function produces the frequency spectra of the bump, and that the peak excitation frequency represents the dominant wavelength. It is evident that the peak excitation frequency from traversing the 2-meter wide bump coincides mainly with the Golden Car unsprung-mass mode. Conversely, frequency response from traversing the wider bump is substantially less intense; some of the excitation frequencies coincide with the Golden Car sprung-mass mode. The wide bump produces hardly any excitation near the unsprung-mass mode.

Depending on the surface treatment, construction type, and traversal speed, profile temporal wavelengths will dominate within a range of frequencies. Furthermore, differences between the suspension responses of the actual vehicle and the Golden Car will result in response sensitivity differences.

[Figure 3 near here].

Figure 4 compares the IRI and RIF-indices from a broad range of bump widths that could dominate an elevation profile. The simulations maintain the same bump height to produce the same excitation intensity at the IRI reference speed. The plots normalize the roughness indices to their maximum values for comparison of their relative wavelength sensitivities.

[Figure 4 near here].

Figure 4(a) shows that both indices characterize roughness from spatial wavelengths up to 2 meters with equal sensitivity. However, the RIF transform extends its sensitivity to characterize roughness from wavelengths beyond that. Figure 4(b) expands the plot of figure 4(a) to compare relative sensitivities at longer wavelengths. Figure 4(c) shows the corresponding R/I factors as a function of bump width. This simulation result demonstrates that for a given vehicle traveling at a fixed speed, the R/I factor differences among roadway segments will correspond to variations in the dominant wavelengths of their surface profile.

2.5 Theory of proportionality trend

Figure 4c indicates that the R/I factors for a Golden Car exhibit distinguishable trends in three regions: I (< 2 meters), II (2 – 40 meters), and III (> 40 meters). Their RIF-index and IRI wavelength sensitivities are identical in region I, and similar in region III. The IRI procedure exhibits maximum sensitivity in region II. The sensitivity differences peak in region II for bump widths of approximately 17-meters. The rapid decrease in R/I factors from a 17-meter wide bump correspond to an increase in the IRI on either side of the R/I slope. This fact establishes a high probability that observing a decrease in the R/I factors among pavement types will correspond to an increase in their respective IRI and vice versa. The authors will refer to this as the *R/I proportionality trend theory*.

3 Case studies

Figure 5 shows roadway level views of each test cell used for this case study.

[Figure 5 near here].

The cells are located at the Minnesota Road Research Facility (MnROAD), which is an outdoor laboratory operated by the Minnesota Department of Transportation in the United States to test the performance of different pavement construction types (MnROAD 2015). Cells C21, C18, and C77, are asphalt constructions. By visual inspection, they appear increasingly rougher in the order shown. The remaining cells are concrete-panel constructions. Cell C36 appears visually smoother than cell C38. The authors used a certified and approved inertial profiler, pictured in lower left of figure 5, to collect elevation profile and vertical acceleration data simultaneously. Applying the IRI transform to the elevation profile samples and the RIF-transform to the vertical acceleration samples produced the IRI and RIF-indices, respectively for a 70-meter section of each cell.

Table 1 summarizes the cell description and the average values of each of the roughness indices. The surface finish for cells 21, 18, and 77 are hot mix asphalt (fractionated recycled asphalt pavement), warm mix asphalt (chip seal), and polymer modified asphalt, respectively. The last two cells are transverse tined 15-feet by 12-feet Portland cement concrete (PCC) panels.

[Table 1 near here].

The mean IRI (I_{80}) derived for the test cells are in units of meters/kilometer (m/km). The mean RIF-indices (R_{80}) are in units of g-force/meter (g/m). The R/I factors are denoted R_{80}/I_{80}. The number of traversals per cell is N. The margin of error in the 95% confidence interval (MOE_{95}) is associated with measurements of the R/I factors.

The MOE percentage for the distribution of random variables within a (1-α)% confidence interval with significance α (Papoulis 1991) is

$$MOE_{1-\alpha} = \pm \frac{\sigma \times t_{1-\alpha/2,df}}{\mu\sqrt{N}} \quad (3)$$

where $t_{1-\alpha/2,df}$ is the *t*-score for a normalized cumulative *t*-distribution with *df* degrees of freedom, μ is the mean, and σ is the standard deviation. Hence, the MOE_{95} is a relative measure of the amount of measurement spread about the mean value.

4 Results and discussion

As shown in figure 6(a), the IRI and the RIF-index agree on the relative roughness differences among the pavements. The figure shows relative changes separately for the asphalt pavements (C21, C18, C77) and the concrete pavements (C36, C38). As shown in figure 6(b), the relative change in R/I factor among the asphalt and the concrete pavements are inversely proportional to their relative changes in roughness. This result is anticipated by the *R/I proportionality trend theory* developed in the previous section. Hence, this result affirms the theoretical expectation that an increase in roughness among pavements will likely correspond to a decrease in their R/I factors. This theory is a byproduct of the fact that the wavelength sensitivity of the IRI procedure varies substantially more than that of the RIF-transform.

[Figure 6 near here].

Testing with the certified and approved inertial profiler imposed a limited number of traversals afforded for each cell. Nevertheless, combining the R/I factors from all five pavements provided a statistically significant sample of 49 data points. Figure 7 plots the

histogram of all the R/I factors. The mean value was 0.128 and the MOE_{95} was 4.68%. The spread includes measurement variations among traversals as well as the effects from variations in the dominant spatial wavelength composition among the profiles.

[Figure 7 near here].

The chi-squared statistic (χ^2) is a method used to test the hypothesis that this distribution is Gaussian (Papoulis 1991). The χ^2 value is

$$\chi^2 = \sum_{k=1}^{n} \frac{(O_k - E_k)^2}{E_k}. \quad (4)$$

The random variables O_k are the histogram values observed in bin k and E_k are the expected values of the hypothesized distribution. The chi-squared test yielded a significance value of 70.5% for the least squares fit of a Gaussian distribution to the histogram. Therefore, the chi-squared tests cannot reject the hypothesis that the R/I factors are normally distributed because the significance value of 70.5% is much greater than 5%.

5 Summary and conclusions

The evolution of connected vehicle methods of roughness characterizations will provide a transformational capable to evaluate network wide roadway performance more frequently. Those characterizations will include all roadway types, including local and unpaved roads. The direct proportionality of the RIF-index to the IRI will provide practitioners with a convenient means of leveraging historical datasets when forecasting long-term deterioration. For example, estimating a future IRI from a future measurement of the RIF-index at the same speed involves simply a division by the R/I factor originally measured. This research demonstrates that the RIF-transform will offer an additional benefit of

characterizing roughness over a broader range of spatial wavelengths than the IRI, and at different speeds that produce g-forces that the rider actually experiences. Case studies of five different pavement types demonstrated that the direct proportionality relationship holds across different surface types.

Statistical testing suggests that the proportionality factors among many pavement types are normally distributed. The case studies demonstrated that the margin of error (in a 95% confidence interval) of proportionality factor measurements diminished to below 5% after only 49 traversals across five different pavement types. This result anticipates that the future use of connected vehicle data to characterize pavement roughness will produce RIF-indices that generally agree with the IRI across pavement types. However, significant differences in the dominant wavelength composition of pavement surfaces will result in differences in their roughness characterizations.

Agencies typically do not characterize the IRI for local and unpaved roads because of the technical and practical limitations of using specialized equipment. Therefore, in future research the authors plan to examine properties of the connected vehicle method when characterizing the ride quality for local and unpaved roads. The future study will include more data collection and associated numerical analysis to characterize trends in the R/I proportionality.

Acknowledgements

A grant from the Mountain Plains Consortium supported this research. The authors also express their sincere appreciation to Mr. Thomas Burchett of Fugro Roadware for his contribution in data collection at MnROAD facilities.

References

Ahlin, K. and Granlund, N.J., 2002. Relating road roughness and vehicle speeds to human whole body vibration and exposure limits. *Int. J. Pavement Eng.,* 3 (4), 207-216.

Akbarian, M., Louhghalam, A., Shetty, S. S., and Ulm, F.-J., 2015. Network Analysis of Virginia's Interstate Pavement-Vehicle Interactions: Mapping of Roughness and Deflection-Induced Excess Fuel Consumption. In: *Proc. 94th Annual Meeting of the Transportation Research Board*, Washington, D.C.

Akinwande, V., Adewole, K., Bello, O., and Akintola, A., 2015. Automatic and Real-Time Pothole Detection and Traffic Monitoring System Using Smartphone Technology. In: *International Conference on Computer Science Research and Innovations (CoSRI 2015)*, Ibadan, Nigeria.

Bilodeau, J.-P., Gagnon, L., and Doré, G., 2015. Assessment of the Relationship between the International Roughness Index and Dynamic Loading of Heavy Vehicles. *Int. J. Pavement Eng.,* DOI:10.1080/10298436.2015.1121780, 1-9.

Bridgelall, R., 2014a. Connected vehicle approach for pavement roughness evaluation. *J. Infrastruct. Syst.,* 20 (1), 1-6.

Bridgelall, R., 2014b. Inertial sensor sample rate selection for ride quality measures. *J. Infrastruct. Syst.,* 21 (2), 1-5.

Bridgelall, R,. 2015a. Precision bounds of pavement distress localization with connected vehicle sensors. *J. Infrastruct. Syst.,*21 (3) 1-7.

Bridgelall, R., 2015b. Precision Bounds of Pavement Deterioration Forecasts from Connected Vehicles. *J. Infrastruct. Syst.,* 21 (1) (1-7).

Bridgelall, R., Tolliver, D. D., Rahman, M. T., and Daleiden, J. F., 2016a. Use of Connected Vehicles to Characterize Ride Quality. *Transp Res Rec.,* 2589, DOI: 10.3141/2589-13, 119-126.

Bridgelall, R., Rahman, M. T., Daleiden, J. F., Tolliver, D. D., 2016b. Error sensitivity of the connected vehicle approach to pavement performance evaluations. *Int. J. Pavement Eng.,* DOI: 10.1080/10298436.2016.1162307, 1-6.

Cruz, J. F. and Castro, J. T., 2015. Estimating road roughness conditions using ubiquitous smartphones and geographic information systems and its application to road network planning in the Philippines. In: Proceedings of the *11th International Conference of the Eastern Asia Society for Transportation Studies (EASTS 2015)*, University of the Philippines, Cebu City, Philippines.

Dawkins, J., Bevly, D., Powell, B., and Bishop, R., 2011. *Investigation of Pavement Maintenance Applications of Intellidrive.* Pooled Fund Study, Charlottesville, Virginia: University of Virginia.

Ghosh, L. E., Lu, L., Ozer, H., Ouyang, Y., and Al-Qadi, I. L., 2015. Effects of Pavement Surface Roughness and Congestion on Expected Freeway Traffic Energy Consumption. In: *The 94th Annual Meeting of the Transportation Research Board*, Washington, D.C.

Gillespie, T. D., Sayers, M. W., and Queiroz, C. A. V., 1986. *The International Road Roughness Experiment: Establishing Correlation and Calibration Standard for Measurement*. The World Bank, Washington, D.C.

González, O. D., 2016. Quantification of the Impact of Roadway Condition on Gas Emissions. In: *The 95th Annual Meeting of the Transportation Research Board*, Washington, D.C.

Islam, S., Buttlar, W.G., Aldunate, R.G., and Vavrik, W.R., 2014. Measurement of pavement roughness using Android-based smartphone application. *Transport Res. Rec.,* (2457), 30-38.

Karamihas, S.M., 2015. *Measuring, Characterizing, and Reporting Pavement Roughness of Low-Speed and Urban Roads.* Research in Progress, Washington, D.C.: Transportation Research Board of the National Academies. Accessed November 1, 2016. http://apps.trb.org/cmsfeed/TRBNetProjectDisplay.asp?ProjectID=3404.

Lak, M.A., Degrande, G., and Lombaert, G., 2011. The influence of the pavement type on ground-borne vibrations due to road traffic. In: G. De Roeck, G. Degrande, G. Lombaert and G. Müller, ed. *Proc. 8th Intl. Conf. on Structural Dynamics.* Leuven, Belgium: EURODYN 2011. 777-784.

Louhghalam, A., Mazdak, T., and Ulm, F-J., 2015. Roughness-Induced Vehicle Energy Dissipation: Statistical Analysis and Scaling. *J Eng Mech* 141(11), 04015046.

Louhghalam, A., Tootkaboni, M., and Ulm, F-J, 2017. Carbon management of infrastructure performance: integrated big data analytics and pavement-vehicle-interactions. *J. Clean Prod* 142, 956-964.

MnROAD, 2015. *Safer, Smarter, Sustainable Pavements Through Innovative Research.* Brochure, Monticello, MN: Minnesota Department of Transportation.

Papagiannakis, A.T., 1997. The Need for a New Pavement Roughness Index; RIDE. *International Truck & Bus Meeting & Exposition.* Washington, D.C.: Society of Automotive Engineers International.

Papoulis, A., 1991. *Probalility, random variables, and stochastic processes.* New York: McGraw-Hill.

Steyn, W. v., Nokes, B., Plessis, L. D., Agacer, R., Burmas, N., and Popescu, L., 2015. Evaluation of The Effect of Rural Road Condition on Agricultural Produce Transportation.. *Transp Res Rec.*, 2473, 33-41.

Yi, C.-W., Chuang, Y.-T., and Nian, C.-S., 2015. Toward Crowdsourcing-Based Road Pavement Monitoring by Mobile Sensing Technologies. *IEEE Trans Intell Transp Syst*, 16 (4), 1905-1917.

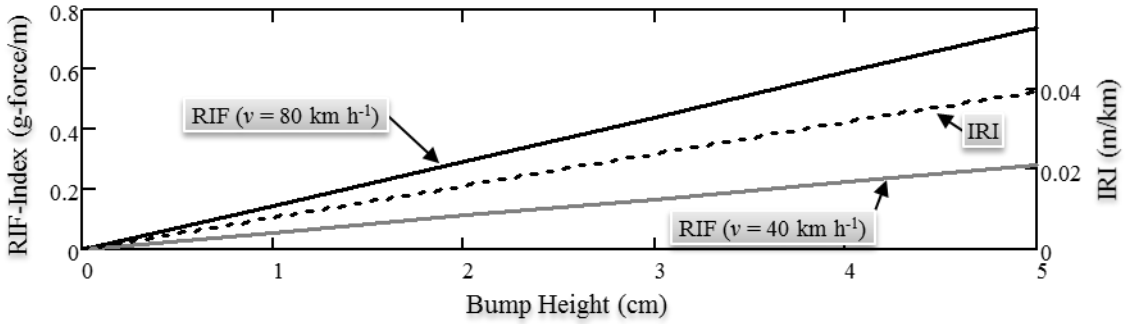

Figure 1. Direct proportionality of the RIF and the IRI as a function of bump intensity.

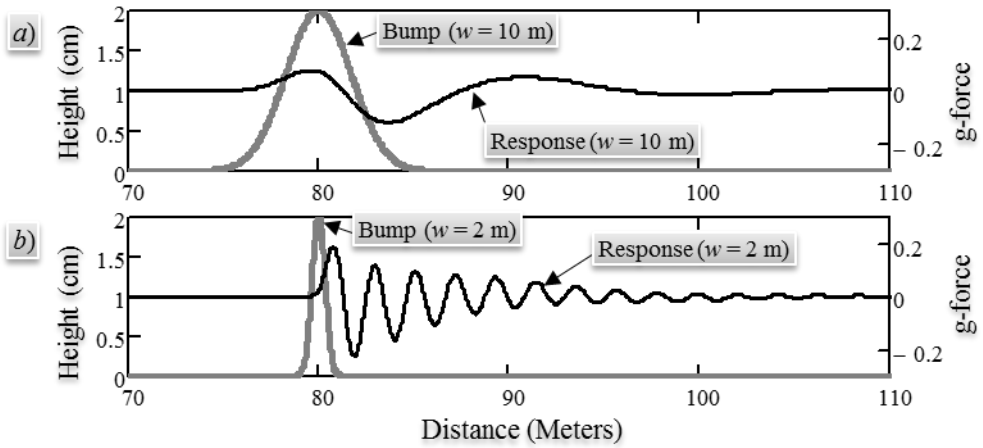

Figure 2. Comparison of Golden-Car inertial responses to (a) wide and (b) narrow bumps.

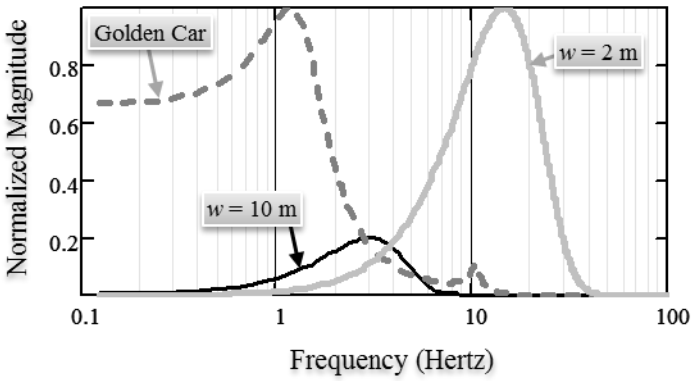

Figure 3. Frequency response of the Golden Car relative to the bump excitations.

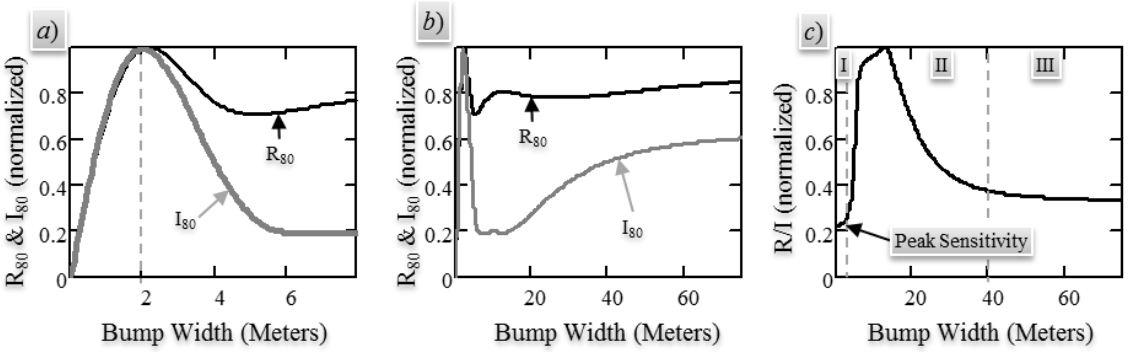

Figure 4. Normalized RIF and IRI transforms of a fixed height bump as a function of bump width.

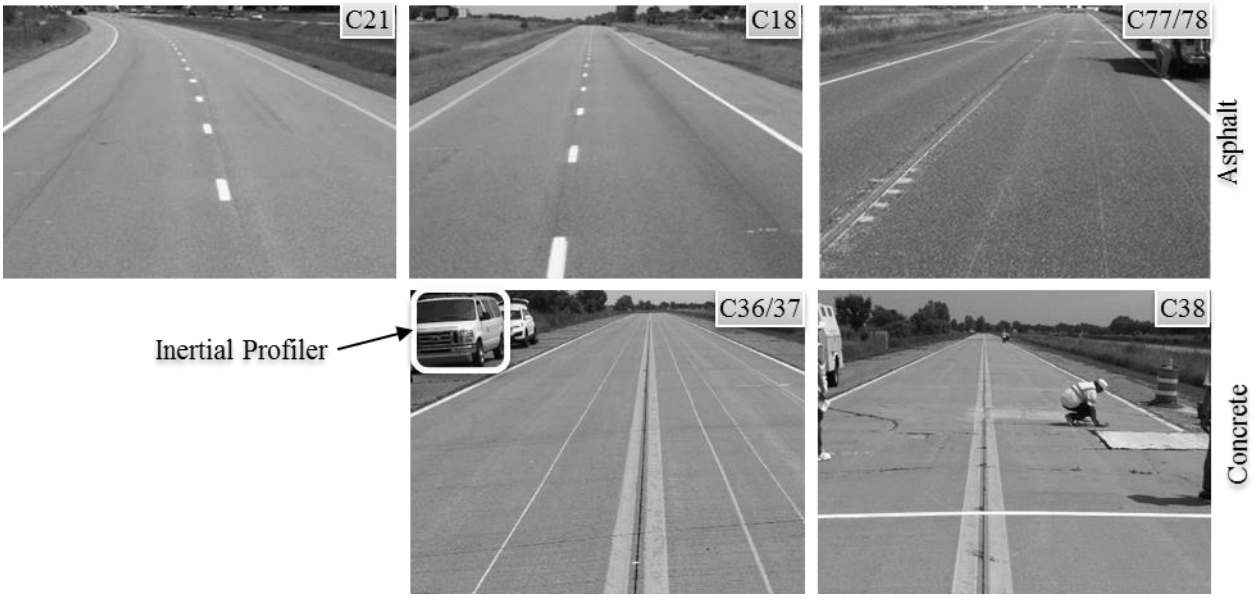

Figure 5. View of each MnROAD test cell and the inertial profiler used.

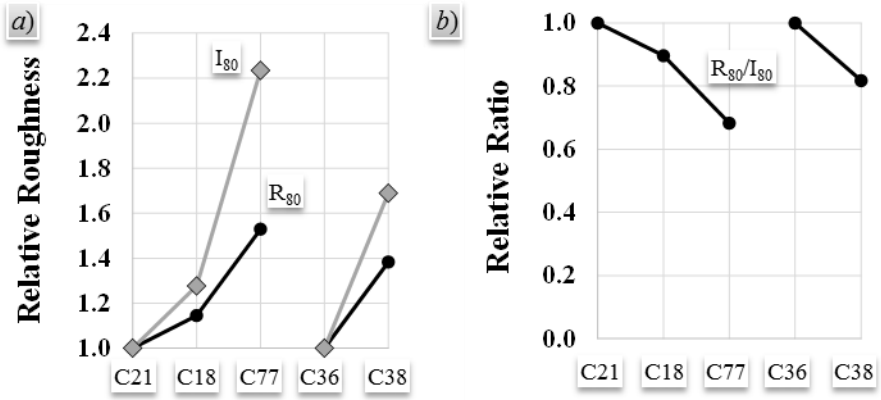

Figure 6. RIF-indices and their position distribution.

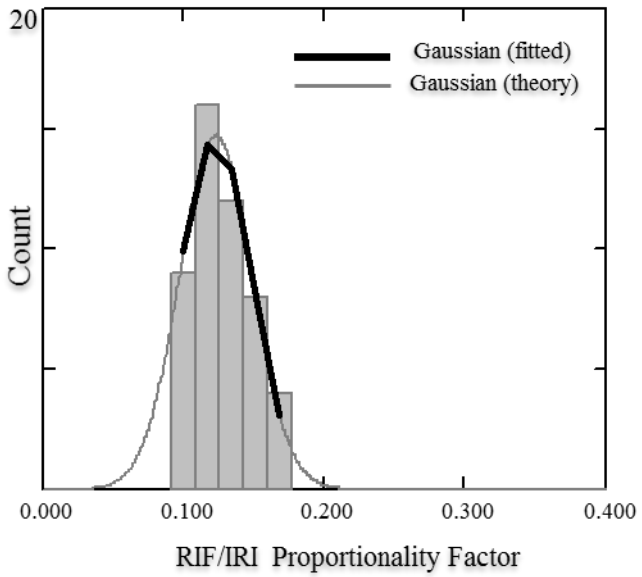

Figure 7. Distribution of R/I factors from five pavement types.

Table 1. Summary of test cells roughness characterizations.

Cell	Description	I_{80} (m/km)	R_{80} (g/m)	R_{80}/I_{80}	N	MOE_{95}
21	Smooth Asphalt	0.770	0.119	0.155	9	7.4%
18	Chip Seal	0.983	0.136	0.139	8	7.8%
77	Rough Asphalt	1.720	0.182	0.106	8	5.9%
36	Smooth Concrete	1.244	0.172	0.138	9	5.9%
38	Rough Concrete	2.101	0.237	0.113	15	4.2%